Changes in Purkinje cell firing and gene expression precede behavioral pathology in a mouse model of SCA2

Stephen T. Hansen[1],[†], Pratap Meera[2],[†], Thomas S. Otis[2] and Stefan M. Pulst[1],*

[1]Department of Neurology, University of Utah, and [2]Department of Neurobiology, University of California Los Angeles, Los Angeles, CA, USA

Spinocerebellar ataxia type 2 (SCA2) is an autosomal dominantly inherited disorder, which is caused by a pathological expansion of a polyglutamine (polyQ) tract in the coding region of the *ATXN2* gene. Like other ataxias, SCA2 most overtly affects Purkinje cells (PCs) in the cerebellum. Using a transgenic mouse model expressing a full-length *ATXN2^Q127*-complementary DNA under control of the Pcp2 promoter (a PC-specific promoter), we examined the time course of behavioral, morphologic, biochemical and physiological changes with particular attention to PC firing in the cerebellar slice. Although motor performance began to deteriorate at 8 weeks of age, reductions in PC number were not seen until after 12 weeks. Decreases in the PC firing frequency first showed at 6 weeks and paralleled deterioration of motor performance with progression of disease. Transcription changes in several PC-specific genes such as *Calb1* and *Pcp2* mirrored the time course of changes in PC physiology with calbindin-28 K changes showing the first small, but significant decreases at 4 weeks. These results emphasize that in this model of SCA2, physiological and behavioral phenotypes precede morphological changes by several weeks and provide a rationale for future studies examining the effects of restoration of firing frequency on motor function and prevention of future loss of PCs.

INTRODUCTION

Background

Spinocerebellar ataxia type 2 (SCA2) is one of the six cerebellar neurodegenerative disorders caused by a mutant polyglutamine (polyQ) protein. In addition to these cerebellar disorders (SCA1, 2, 3, 6, 7 and 17), Huntington disease, dentatorubral-pallidoluysian atrophy and spinal bulbar muscular atrophy (SBMA) are also polyQ disorders, but affect primarily other neuronal groups. These disorders all show autosomal dominant inheritance and are caused by expansion of a CAG DNA repeat in the coding region of the respective gene. In SCA2, these excessive CAG repeats in exon 1 of the *ATXN2* gene cause expansion of a polyQ domain in the protein ataxin-2 (ATXN2). As in the other polyQ disease, the size of the polyQ repeat is inversely associated with age of onset (AO)

in SCA2 ([1],[2]). Evidence suggests polyglutamine disorders exert their pathology through a toxic gain of function of the protein and larger polyQ expansions have been associated with greater pathology along with an earlier AO of motor deficits, although this is subject to variability ([3]). *ATXN1*, is widely expressed in the brain ([4],[5]); however, neurodegeneration is limited to cerebellar PCs, and neurons in the brainstem and spinal cord ([6]). As with most autosomal dominant ataxias, symptoms are characterized by a progressive loss of motor coordination, neuropathies, slurred speech, cognitive impairment and loss of other functional abilities arising from deep cerebellar nuclei ([7]).

ATXN2 is widely expressed in the mammalian nervous system ([1],[8],[9]). It is known to associate with the endoplasmic reticulum ([10]), the Golgi complex ([11]) and has been

---

*To whom correspondence should be addressed at: 175 N. Medical Dr., 5th floor, Salt Lake City, UT 84312, USA. Fax: +1 8015855083;
Email: stefan.pulst@hsc.utah.edu
†These two authors contributed equally.

implicated in messenger RNA (mRNA) translation and transport ([12]). Other data suggest that *ATXN2* may be an important component of energy metabolism and weight regulation. For example knockout (KO) mouse models of *ATXN2* develop obesity ([13],[14]). *ATXN2* orthologs have been suggested to be involved in long-term habituation at the synapse in fruit flies ([15]). Work in the *Caenorhabditis elegans* model continues to support ATXN2's function in translational regulation ([16]), as well as embryonic development ([13]). Furthermore, ATXN2 is a known to interact with the poly-A binding protein 1 and assemble with polyribosomes, which implicates ATXN2 as being involved in the metabolism of RNA ([17]). Emerging evidence suggests that ATXN2 may also be involved in endocytosis and epidermal growth factor receptor trafficking ([18]) as well as actin filament formation ([19]).

The AO of SCA2 symptoms exhibits an inverse correlation to the number of glutamine repeats. Recent work has reported that glutamine expansions in the C-terminal domain of the *CACNA1a* gene, which codes for the voltage-activated calcium channel Ca$_v$2.1, may interact with *ATXN2* and accelerate the AO of the disease ([2]). Despite this relative wealth of information regarding the normal function of ataxin-2, little is known about whether the expansion of the polyQ domain leads to a gain of normal function or gain of a novel toxic function.

Relatively little is known about the early cellular events and physiological changes induced by mutant polyQ proteins in the cerebellum. PCs in the cerebellum receive input from the two major afferent pathways to the cerebellum, the climbing fiber and mossy/parallel fiber pathways. Climbing fibers from the inferior olive synapse in a one-to-one fashion onto PCs, whereas mossy fibers synapse on granule cells which, in turn, give rise to parallel fiber axons that converge massively (100 000 to 1) onto PC dendrites ([20]). PCs exhibit tonic action potential firing due to intrinsic pacemaking ([21]); they are also excited by parallel and climbing fiber input. PCs are the only output from the cerebellar cortex and they project to and inhibit deep cerebellar nuclear neurons. Studies of mutations in specific genes causal in human ataxias have provided differing results with regard to the PC spiking frequency and the persistence and regularity of their tonic firing ([22]–[24]).

We previously reported on a transgenic mouse model of SCA2, which targeted the expression of a full-length-mutant *ATXN2*^{Q58} complementary DNA (cDNA) to PCs using the Purkinje cell protein-2 (Pcp2) promoter ([25]). This model showed a late-onset progressive motor phenotype accompanied by the formation of diffuse cytoplasmic aggregates. Although actual cell loss of PCs was relatively minor even at 12 months, shrinkage of the molecular layer and reduction of calbindin staining in PCs and dendrites were observed earlier.

By using a longer polyglutamine repeat, we have now generated an SCA2 mouse model that shows a more clearly defined phenotype along with an earlier degenerative onset. Using this model, we investigated early changes in biochemical and cellular functions of PCs. In particular, we sought to examine the interplay between PC dysfunction in the slice, changes in gene expression, reduction in the molecular layer size and in PC number and the resulting effects on motor behavior.
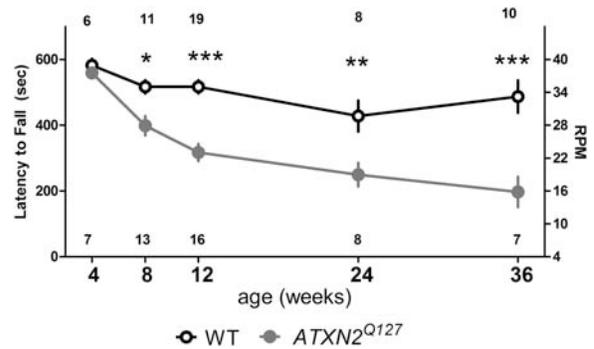

Figure 1. Progressive deterioration of motor performance on the accelerating rotarod beginning after 4 weeks of age. Latency to fall off the accelerating rotarod (left *Y*-axis) and RPMs (right *Y*-axis) data for *ATXN2*^{Q127} (gray circle) and WT animals (white circle). Data represent the mean $\pm$ SEM of three trials on the test day. Number of animals tested for WT and *ATXN2*^{Q127} animals are listed above and below, respectively. Two-way ANOVA comparing the age × genotype; Bonferroni *post-hoc* tests. *$P <$ 0.5, **$P <$ 0.01, ***$P <$ 0.001. Error bars represent $\pm$ SEM.

RESULTS

Ataxin-2-mutant mice exhibit an early pathological motor phenotype

SCAs commonly show disease onset in early adulthood with progressive worsening of symptoms with age. In modeling the human SCA2 phenotype, we therefore sought to recapitulate normal motor function in young animals followed by a progressive deficit with age. Indeed, *ATXN2*^{Q127} mice at 4 weeks performed similar to wild-type (WT) littermates on the accelerating rotarod (Fig. [1]). With age, however, *ATXN2*^{Q127}-mutant mice demonstrated a progressive decline in motor performance. Two-way analysis of variance (ANOVA) determined that *ATXN2*^{Q127} mice exhibited a significant age-related decrease of motor performance. Significant main effects were detected for genotype ($F = 54.5_{1,107}$), age ($F = 15.2_{4,107}$) and an interaction of genotype × age ($F = 4.1_{4,107}$). Bonferroni *post-hoc* tests revealed no significant difference between genotypes at 4 weeks of age. However, statistically significant differences emerged as early as 8 weeks ($P < 0.05$), and increased at ages 12 ($P < 0.001$), 24 ($P < 0.0001$) and 36 ($P < 0.001$) weeks. Thus, motor behavior was normal from birth to 4 weeks, showed minor, but significant impairment by 8 weeks, which then progressively worsened over the ensuing 28 weeks.

Mutant ataxin-2 expression results in a loss of molecular layer volume and aggregate formation in cerebellar Purkinje cells

Along with the overt motor phenotype, we observed anatomical abnormalities associated with expression of the transgene in mutant mice, although at latter ages. Figure [2]A–J shows representative images of WT (top row) and *ATXN2*^{Q127} cerebellar sections (bottom row) across five different age points (columns). Two-way ANOVA detected a significant main effect of genotype ($F = 47.2_{1, 20}$). Bonferroni p*ost-hoc* tests determined that mutant animals at 12 ($P < 0.05$), 24 ($P < 0.01$) and 40 ($P < 0.001$) weeks of age exhibited a significant
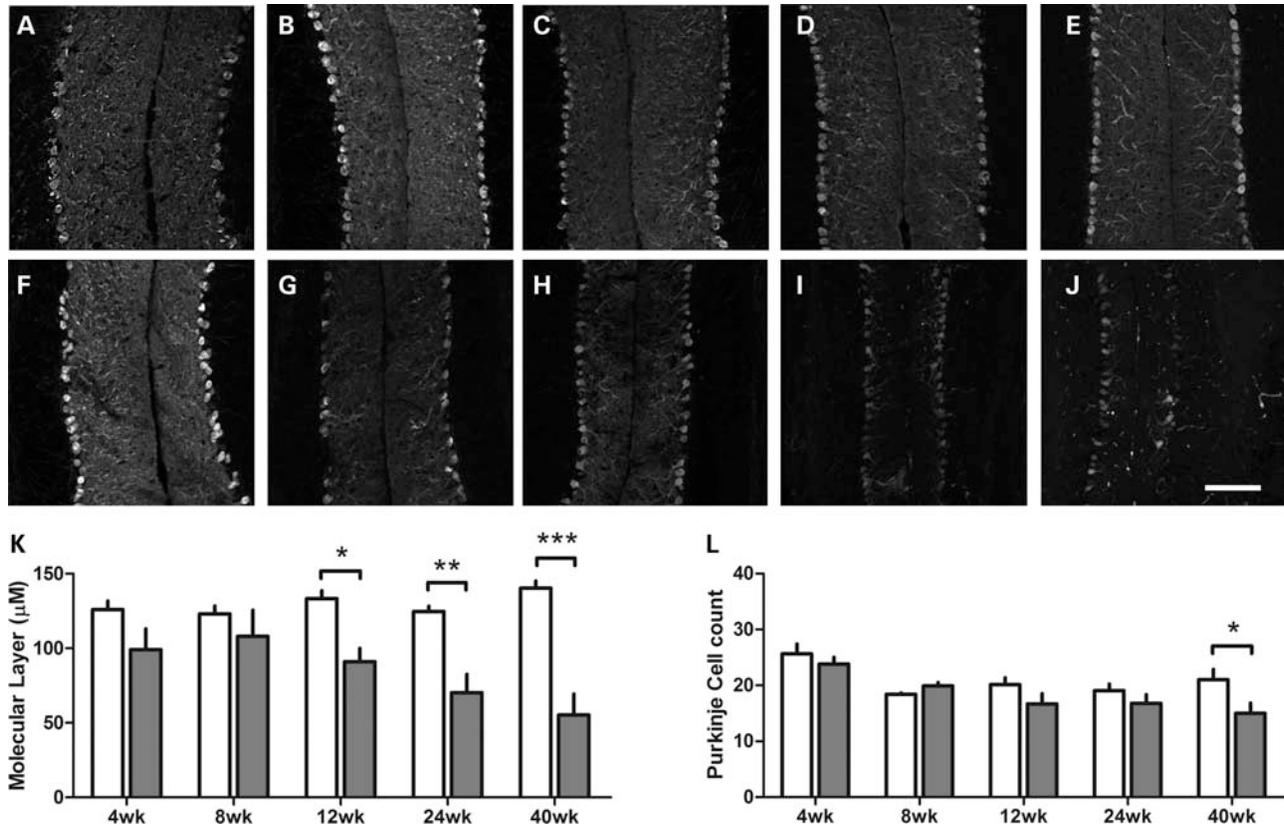
Figure 2. Changes in PC number and molecular layer thickness occur late in $ATXN2^{Q127}$ mice. Representative confocal images stained for calbindin 28-k from the 'fissura prima' of the cerebellar vermis: WT animals (**A–E**) and $ATXN2^{Q127}$ transgenic mice (**F–J**) at 4, 8, 12 and 24 weeks of age are shown. (**K**) Graphical representation of changes in the molecular layer thickness. (**L**) PC count of $ATXN2^{Q127}$ (gray bars) and WT (white bars) animals across age. $N = 2-3$ animals for each category. Two-way ANOVA comparing the age × genotype; Bonferroni *post-hoc* tests. $^*P < 0.05$; $^{**}P < 0.01$; $^{***}P < 0.001$. Error bars represent ± SEM. Scale bar = 200 μM

loss of molecular layer thickness (Fig. 2K). Overall cell loss in $ATXN2^{Q127}$ animals exhibited a significant main effect of genotype ($F = 7.16_{1,\ 20}$). Bonferroni *post-hoc* tests indicated that only 40-week-old $ATXN2^{Q127}$ differed from WT (Fig. 2L). Despite normal motor behavior at the age of 4 weeks, perinuclear ataxin-2 aggregates were already detectable at that time in some PCs with an antibody targeting an epitope shared by human and mouse ATXN2 (Fig. 3). The number of PCs showing inclusions and the size of inclusions increased with age, whereas diffuse cytoplasmic staining became nearly undetectable at advanced ages.

Deficits in cerebellar gene expression precede motor phenotype and anatomical degeneration in ATXN2^{Q127}-mutant animals

To examine changes in gene expression, we focused on genes known to be specifically expressed in PCs such as *Calb1* (encoding calbindin 28K) and *Pcp2* (encoding PC protein 2) and several additional genes the expression of which is enriched in but not exclusive to PCs (Fig. 4). This experimental design allows comparison between the WT and transgenic animal expression within a given time point, but not across different time points. Additionally, we tested age points at which no significant loss of PC bodies was detected. At

postnatal day 1, $ATXN2^{Q127}$ and WT animals exhibited similar gene expression (data not shown). As early as 4 weeks, $ATXN2^{Q127}$ animals exhibited a modest, yet statistically significant reduction in the expression of *Calb1* ($P < 0.05$), whereas all other genes tested remained unchanged from WT (Fig. 4A). At 8 weeks of age, quantitative polymerase chain reaction (qPCR) analysis of $ATXN2^{Q127}$ mice confirmed the trend of decreased *Calb1* expression ($P < 0.001$) as well as a significant reduction in *Pcp2* ($P < 0.01$), *Grid2* ($P < 0.001$) and *Grm1* ($P < 0.05$) expression (Fig. 4B). The gene expression changes continued at 12 weeks of age (Fig. 4C). By 24 weeks, a reduced expression in *Itpr1* ($P < 0.05$) was detected for the first time (Fig. 4D). The qPCR data displayed here also indicate that across all ages mouse ataxin-2 (m*Atxn2*) remained unchanged throughout the study and in fact mutant mice displayed a modest, but non-significant, increase in m*Atxn2* expression. The human *ATXN2*-mutant transgene is also present in $ATXN2^{Q127}$ animals, as would be expected, and although variability existed between ages, expression remained similar across all ages of mice tested. In summary, qPCR data demonstrated that PC-specific genes showed a differential reduction in expression, which was progressive with time. However, even among the few genes tested by qPCR, the reduction in expression was not global. *Cacna1a* did not change significantly and *Itpr1* only at 24 weeks. On the
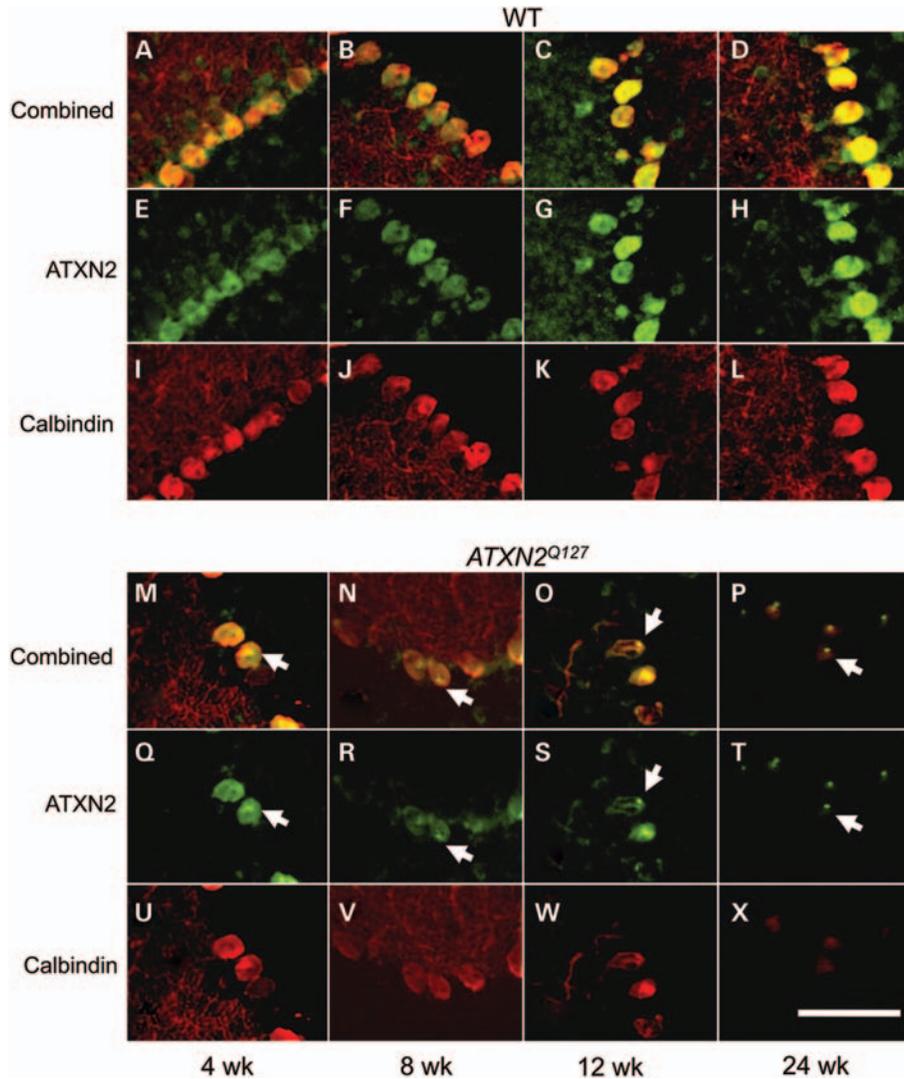
Figure 3. Ataxin-2 aggregates detected in mutant mice. As early as 4 weeks, occasional PCs show perinuclear aggregates. Note that at 24 weeks only aggregates remain visible. Representative immunohistochemical images from combined double staining for WT (**A–D**) and *ATXN2*^{Q127} (**E–H**) mice. Antibodies directed against calbindin 28-k (red) and ataxin-2 (green) detected the presence of aggregate formations (white arrows) in *ATXN2*^{Q127} animals across all age points. All images for a respective antibody were taken at the same exposure times. Scale bar = 100 μM

other hand, reduction of *Calb1* preceded loss of molecular layer thickness by several weeks.

Electrophysiological behavior of Purkinje cells in mutant mice

We decided to investigate whether physiological functional changes in PCs correlated with the ataxic phenotype of our *ATXN2*^{Q127} mouse model seen in the accelerated rotorod behavior (see Fig. 1). We exploited the fact that normal healthy PCs exhibit intrinsically generated, regular firing (21,26), and used a noninvasive extracellular recording technique to study PC firing in cerebellar slices at different ages (4–40 weeks) in WT and *ATXN2*^{Q127} mice at a near physiological temperature of 34.5 ± 1°C.

Representative traces of both WT and *ATXN2*^{Q127} mice from each age group investigated are presented in Figure 5. Each panel shows recording data from one second in time

and includes as an inset a histogram of all interspike intervals (ISI) in a 2 min recording period from that PC. The mean firing frequency and the coefficient of variation of the ISI are indicated in each inset. These data from individual PCs highlight a marked slowing in the firing rate with age in the *ATXN2*^{Q127} mice.

In WT animals, each PC fires at a characteristic rate (21). To document the average firing behavior of the population of PCs, the mean firing frequency was calculated over 2 min epochs for each PC and population distributions of these mean values are plotted in Figure 6 for each age group and genotype. The mean firing frequencies from 6 to 40 weeks are unchanged in the WT, whereas in the *ATXN2*^{Q127} mice over the same age range the distributions progressively shift to slower firing frequency.

Figure 7 summarizes the average firing frequency, regularity of firing and fraction of cells firing regularly as a function of age and genotype. In WT PCs, we saw an initial increase in
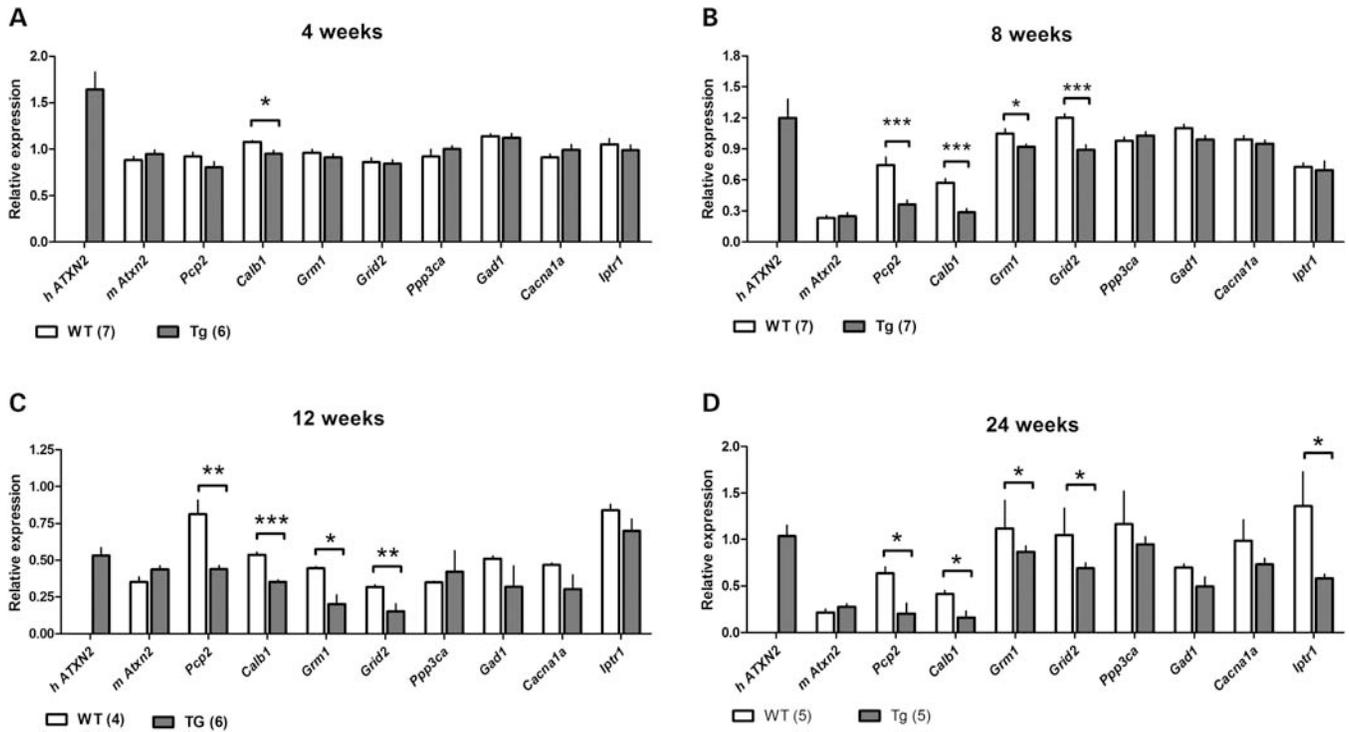
Figure 4. Early expression changes of key cerebellar genes including several PC-specific genes at four time points. Significant reductions in four genes are seen at 8 weeks, but not 4 weeks except for a minor reduction in calbindin mRNA levels. Quantitative PCR data from mouse cerebella comparing PC-specific gene expression of $ATXN2^{Q127}$ (gray bars) and WT animals (white bars) (**A–D**). Genes tested: human transgene (h $ATXN2$), mouse ataxin-2 (m$Atxn2$), PC protein 2 ($Pcp2$), calbindin 28-k ($Calb1$), metabotropic glutamate receptor 1 ($Grm1$), glutamate receptor ionotropic delta-2 ($Grid2$), calcineurin ($Ppp3ca$), glutamate decarboxylase ($Gad1$), voltage-gated calcium channel Ca$_v$2.1 ($Cacna1a$), inositol triphosphate receptor 1 ($Itpr1$). N, size for each genotype and age group is listed in brackets. Gene expression normalized to the $Wasf1$ housekeeping gene. Student's two-tailed t-test compared $ATXN2^{Q127}$ with WT gene expression in each age group. $^*P < 0.05$, $^{**}P < 0.01$, $^{***}P < 0.001$. Error bars represent $\pm$ SEM.

the mean firing frequency during maturation from 30 ± 1 Hz ($n = 120$) at 4 to 42 ± 1 Hz ($n = 72$) at 6 weeks, after which it remained essentially constant ($\sim$45 Hz) from 6 to 40 weeks of age. In contrast, the firing rate of PCs measured in $ATXN2^{Q127}$ mice progressively declined (from 35 at 6– 11 Hz at 40 weeks) (Fig. 7A). Two-way ANOVA revealed the main effects of genotype ($F = 246.6_{1,976}$), age ($F = 10.8_{5,976}$) and genotype × age ($F = 42.7_{5,976}$). The Bonferroni *post-hoc* test showed that WT and $ATXN2^{Q127}$ groups were not significantly different at 4 weeks, first became statistically different at 6 weeks ($P = 0.015$) and remained significantly different at 8 ($P = 0.000024$), 12, 24 and 40 weeks (all $P < 8 \times 10^{-7}$).

The majority of PCs fired regularly and we observed only a very small fraction of bursting cells which showed no differences between the WT and transgenic groups (Fig. 7B). We quantified the regularity of firing by calculating the coefficient of variation of adjacent spikes (27), an index for which higher values indicate less regular firing. In WT PCs, there is a small increase in firing variability from 12 to 40 weeks. Despite the marked decrease in firing frequency, the firing regularity remained remarkably constant in $ATXN2^{Q127}$mice and no statistically significant differences were observed for age or genotype (two-way ANOVA, Fig. 7C).

Rbfox1-mediated splicing is not altered in mutant mice

ATXN2 is known to interact with Rbfox1 (28) and PC-specific deletion of Rbfox1 and Rbfox 2 results in splicing

abnormalities in several genes, including ion channel-forming genes in PCs (29). Here, we sought to examine whether the mutant transgene resulted in changes in the relative abundance of splice variants in channel-forming genes which may account for the reduction in endogenous PC firing frequency. We performed RT-PCR on samples from both young (4 weeks) and older (24 weeks) WT and mutant mice (Fig. 8). No alternative splice differences were detected between $ATXN2^{Q127}$ mice and WT litter mate samples in any of the three Ca^{2+} channels: *Cacna1B*, *Cacna1D* and *Cacna1S* (Fig. 8). Interestingly, *Cacna1S* failed to amplify any product for 4-week-old mice. *Cacna1B* primers were designed to amplify two bands corresponding to 235 and 172 bp. In this case, a ratio was taken from the intensity signal of the upper and lower bands (Table 1). The ratios were log transformed and averaged followed by a two-tailed paired t-test. No difference was statistically observed between genotypes ($P > 0.05$). Two genes encoding for K$^+$ channels, *Kcnd3* and *Kcnq2*, also failed to indicate differences in splice variants between $ATXN2^{Q127}$ and WT samples. Like the aforementioned *Cacna1B*, both the K$^+$ channel primer sets also amplified two endogenous bands. *Kcnd3* primers amplified two bands at 233 and 166 bp respectively. In 24-week-old animals, the larger band appeared to be preferentially amplified regardless of the genotype. No such distinction between the upper and lower bands was present in 4-week-old samples. *Kcnq2* also amplified two bands of 227 and 197 bp in length. In both 4- and 24-week-old animals, there appeared a preferential
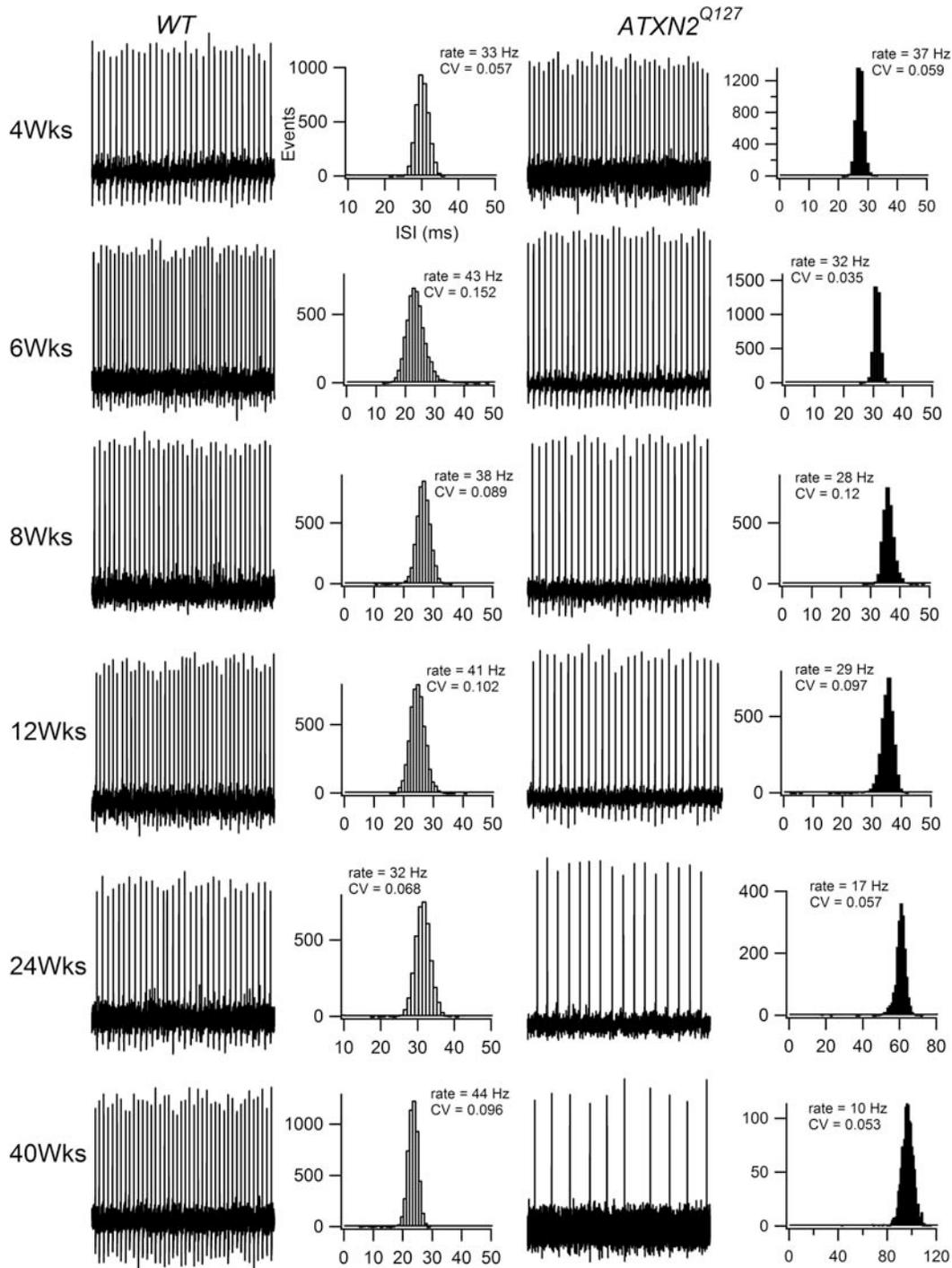
Figure 5. PC firing rate remains constant in WT but progressively decreases with age in *ATXN2*^{Q127} mice. To the left of each panel are examples of extracellular recordings from PCs at the indicated ages in WT and transgenic *ATXN2*^{Q127} mice. These one second traces show that firing decreases progressively with age in the transgenic (*ATXN2*^{Q127}) but not WT mice. To the right of each panel are histograms of inter spike intervals for the 2 min recording periods from the same neuron. Indicated on each histogram are the mean firing rate and the local coefficient of variation (CV). All recordings were made at $34.5 \pm 1°C$ and the experimenter was blinded to the genotype.

amplification of the larger band. As with the previous *Cacna1B* assay, a *t*-test on log-transformed *Kcnq2* data failed to detect a statistically significant difference in band intensity when comparing across genotypes ($P > 0.05$). Finally, we looked for mutually exclusive splice variants in the *Scn8a*

gene encoding for transmembrane portions of the sodium channel Na$_v$1.6. Here, we looked both at *Scn8a* (5) with primers targeted to exon 5, which is responsible for encoding the S3–S4 segment of domain I. We observed only the presence of the upper band in both genotypes at both ages.
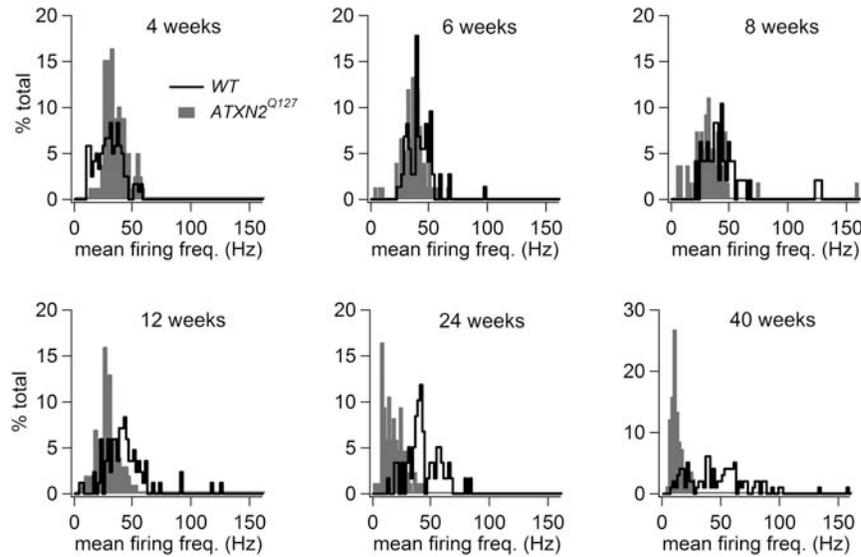
Figure 6. Population distributions of the mean PC firing rate show a shift towards slower firing with age in SCA2^{Q127} mice. Each histogram displays the distribution of mean firing rates of WT (black traces) and *ATXN2^{Q127}* PCs (gray filled traces) with the *y*-axis indicating the percent of total PCs recorded. The numbers of recorded PCs are 4 weeks: 120 WT, 79 *ATXN2^{Q127}*; 6 weeks: 73 WT, 75 *ATXN2^{Q127}*; 8 weeks: 48 WT, 54 *ATXN2^{Q127}*; 12 weeks: 84 WT, 100 *ATXN2^{Q127}*; 24 weeks: 59 WT, 85 *ATXN2^{Q127}*; 40 weeks: 98 WT, 82 *ATXN2^{Q127}*.
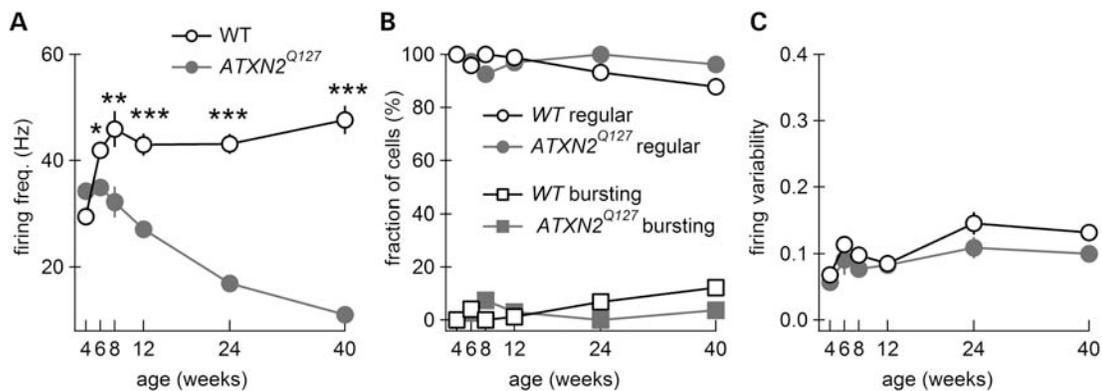

Figure 7. Mean firing rate in PCs decreases but firing variability and fraction of regularly firing cells are unchanged in *ATXN2^{Q127}* mice. (**A**) The mean frequency values in Hertz, shown in black line white circle for WT at 4, 6, 8, 12, 24 and 40 weeks, are 30 ± 1 ($n = 120$), 42 ± 1 ($n = 73$), 46 ± 3 ($n = 48$), 43 ± 2 ($n = 84$), 43 ± 2 ($n = 59$) and 48 ± 3 ($n = 98$), respectively. Significantly reduced PC firing frequency is already evident in *ATXN2^{Q127}* mice as early as 8 weeks of age and subsequently worsens. The mean values in Hertz for *ATXN2^{Q127}* PCs shown in gray are 34 ± 0.9 ($n = 79$), 35 ± 1 ($n = 75$), 32 ± 3 (54), 27 ± 1 ($n = 100$), 17 ± 1 ($n = 85$) and 11 ± 1 ($n = 82$) at 4, 6, 8, 12, 24 and 40 weeks, respectively. (**B**) The fraction of cells that show bursting behavior is low and does not differ significantly between the WT and *ATXN2^{Q127}* groups. (**C**) The coefficient of variation of adjacent intervals, a measure of the regularity of firing, is not significantly changed between WT and *ATXN2^{Q127}* mice. The firing variability values for control mice at different age groups are 0.068 ± 0.0003, 0.114 ± 0.009, 0.098 ± 0.009, 0.085 ± 0.005, 0.146 ± 0.017 and 0.132 ± 0.01 at 4, 6, 8, 12, 24 and 40 weeks, respectively, versus 0.057 ± 0.005, 0.091 ± 0.023, 0.077 ± 0.008, 0.083 ± 0.006, 0.109 ± 0.016 and 0.1 ± 0.01 in SCA2 transgenic mice at the same age group, respectively. Data in (A) and (C) are expressed in mean $\pm$ SEM. Two-way ANOVA comparing age $\times$ genotype followed by Bonferroni *post-hoc* tests yielded *P*-values indicating significant differences between WT and *ATXN2^{Q127}* mice: *$*P = 0.015$, **$**P = 0.00024$ and ***$***P < 8 \times 10^{-7}$.

Additionally, we looked at *Scn8a* (*18*) on exon 18, which encodes for the S3–S4 segment of domain III of the membrane spanning protein. Here, again we observed only the presence of the larger band.

DISCUSSION

We present evidence of early endophenotypic markers associated with pathological expansion of the polyglutamine tract in *ATXN2* in a new mouse model of SCA2. By collecting biochemical, electrophysiological and behavioral data across a wide range of ages, from presymptomatic to late stages, we have obtained a comprehensive picture of disease progression. The first observable changes occurred at 4 weeks and were biochemical, and these were followed by changes in the electrophysiological behavior of PCs which were statistically significant at 6 weeks. Finally, deficits in motor behavior became significant at 8 weeks. Biochemical, electrophysiological and behavioral deficits worsened over the period between 8 and 40 weeks but PC cell loss was not apparent until 40 weeks.
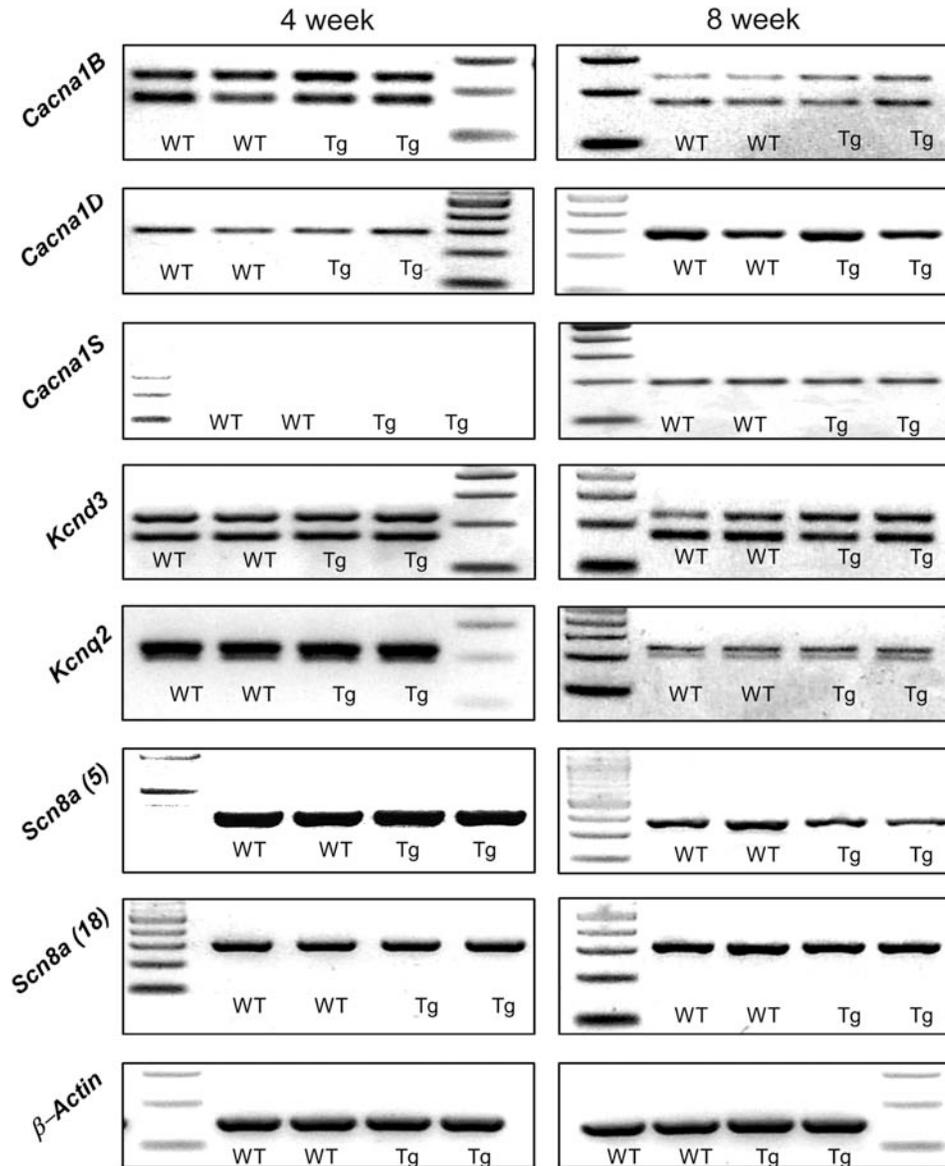
Figure 8. RT-PCR for Rbfox1-mediated alternative splice variants. RT-PCR gel images of alternative splice sights in channel-forming genes. Two age points (4 weeks: left column; 24 weeks: right column) were tested. WT = wild type, Tg = *Atxn2^{Q127}*. Voltage-dependent calcium channels: Ca$_v$2.2 (*Cacna1B*), Ca$_v$1.3 (*Cacna1D*), Ca$_v$1.1 (*Cacna1s*). Voltage-gated potassium channels: K$_v$4.3 (*Kcnd3*), K$_v$7.2 (*Kcnq2*). Voltage-gated sodium channel Na$_v$1.6: exon 5 (*Scn8a (5)*), exon 18 (*Scn8a (18)*).

Taken together, these data suggest a sequence of events in which concerted biochemical dysregulation leads to impairment of the basic electrophysiological function of PCs and this contributes to ataxic symptoms.

In this study, we characterized the effects of a transgene expressing a full-length cDNA construct with a long uninterrupted CAG repeat. In a prior study, we had examined the effects of a full-length transgene with 58 CAG repeats, again using the Pcp2 promoter (25). Consistent with studies in SCA2 patients, AO was much earlier in the ATXN2^{Q127} line than in the ATXN2^{Q58} line (1,2). During the study of the ATXN2^{Q58} mouse model, we also had generated two lines expressing a human *ATXN2* cDNA encoding Q22, the most common normal allele in human populations. These

ATXN2^{Q22} lines expressed the transgene at similar levels as the ATXN2^{Q58} lines, but did not show motor or anatomical phenotypes at 12 months of age and were subsequently terminated. Despite the absence of changes in cerebellar morphology or rotarod performance, we cannot exclude that studies at the transcriptome or single cell level would have revealed subtle changes or that changes would have occurred at 18 or 24 months of age.

At the biochemical level, we observed progressive declines in a number of PC-enriched gene products which in some cases preceded cell loss. For example, mRNA levels of the intracellular calcium-regulating gene, *Calb1*, were normal at birth, significantly downregulated as early as 4 weeks of age, and exhibited a continual decline of expression at ages

Table 1. RT-PCR splice variant ratios. Band intensity values for both 4- and 24-week-old WT ($N = 3$) and Tg ($N = 3$) animals. Data represent the ratio of the upper band to the lower band mean of sample repeated in triplicate. A paired two-tailed T-test on log-transformed data did not detect any significant differences between genotypes for any gene at either age ($P > 0.05$). Voltage-gated calcium channel $Ca_v2.2$ (*Cacna1B*), voltage-gated potassium channel $K_v4.3$ (*Kcnd3*), voltage-gated potassium channel $K_v7.2$ (*Kcnq2*).

| | *Cacna1B* | | *Kcnd3* | | *Kcnq2* | |
	4 week	24 week	4 week	24 week	4 week	24 week
WT	0.885	0.930	0.970	1.168	1.168	1.438
WT	0.873	0.912	0.990	1.200	1.223	1.594
WT	0.861	0.923	0.972	1.203	1.091	2.011
Tg	0.871	0.930	0.918	1.189	1.247	1.686
Tg	0.837	0.917	0.981	1.179	1.118	1.509
Tg	0.824	0.999	0.936	1.117	1.287	1.774

older than 4 weeks. A reduced expression of *Calb1* was followed by a significant reduction in *Pcp2*, *Grm1* and *Grid2* expression at 8 weeks, each of which also demonstrated a progressive diminished expression with age. The reduced expression of these genes was not a function of PC death, as number of PCs between WT and $ATXN2^{Q127}$ remained relatively constant until 40 weeks of age.

Consistent with our findings, mouse strains in which these genes are deleted show ataxic phenotypes. Calbindin 28-K null mice exhibit normal nervous system development and cerebellar histology, but these mice go on to develop impairments in motor performance linked with alterations in synaptic calcium currents (30). Calbindin and parvalbumin reductions have also been described in SCA1-mutant mice and the loss of calcium buffering capacity has been suggested to contribute to pathology (31). However, there is a debate as to whether elevated calcium is a primary contributor to subsequent PC loss and ataxic behavior (32).

Abnormalities in handling of calcium fluxes have been implicated in neurodegeneration in general (for reviews, see 33 and 34) and within the family of trinucleotide repeat disorders (35–39). In human ataxia patients, a normal variation in the polyQ repeat in *Cacna1a* ($Ca_v2.1$) modifies the AO in SCA2 patients (2). *Cacna1a* expression, however, was not altered in our SCA2 mouse model until very late in the disease, and even then reduction did not reach significance and may have been solely due to loss of PCs at that stage. Mutant ATXN2 protein physically interacts with the IP_3 receptor (IP3R1) and leads to enhanced calcium release from intracellular stores upon mGluR1 stimulation (36). Dysregulation or mutation of IP3R1 may also be important in other SCAs (40). Slight decreases in the expression of *Grm1*, the gene encoding mGluR1, were seen beginning at 8 weeks in transgenic animals, whereas changes in *Itpr1* expression occurred later and only reached significance at 24 weeks.

The downregulation of *Grid2* and *Grm1* early in the disease process may in itself hasten dysfunction and degeneration *in vivo*. Mutant mGluR1 KO mice display cerebellar ataxia along with impaired motor learning and loss of long-term depression (41). Abnormal calcium handling in the early stages of SCA2 pathogenesis may be further aggravated by reduction in *Calb1* expression and calbindin-28K protein levels. In our model, reduction of *Calb1* as measured by

qPCR preceded the onset of physiologic abnormalities by 2 weeks and of behavioral abnormalities by 4 weeks and worsened with disease progression.

Grid2 is localized to the PC-parallel fiber synapse and is reported to be involved in the maintenance of synapse integrity, as well as long-term depression. Importantly, *Grid2* is also involved in cerebellar motor coordination and learning (for review, see 42). Alterations in *Grid2* expression have also been linked to ataxic phenotypes and loss of PCs. Mutations in the N-terminal domain of *Grid2*, the *hotfoot* allele, lead to ataxia of the hindlimbs in mice (43). Lurcher mice express a lethal point mutation in the *Grid2* gene, resulting in excitotoxic apoptosis of PCs (44, reviewed in 45).

Using a noninvasive recording technique, we measured PC firing in WT and $ATXN2^{Q127}$ mice from 4 weeks until 40 weeks of age. In WT mice, at 4 weeks of age, the mean PC firing frequency was 30 Hz ($n = 120$) and climbed to ~45 Hz at 6weeks and remained essentially unaltered across the age range studied. By comparison, in $ATXN2^{Q127}$ mice, the mean PC firing frequency was identical to WT at 4 weeks but began to decline and was significantly lower at 6 weeks. The firing rate declined progressively, such that at 40 weeks PCs fired on average at ~25% the WT rate. These physiological data correlate with the rotarod behavior which shows no evidence of impairment at early ages but progressively worsens over a similar age range.

Despite this striking reduction in firing frequency, PCs maintained highly regular firing patterns as indicated by the low fraction of cells that exhibited bursting and the low coefficient of variations (CVs). The lack of impairment in regularity is in contrast to reports on mouse models of episodic ataxia type 2 (EA-2), in which PC firing becomes more variable and normalization of this variability reduces ataxic behavioral symptoms (24). The maintained precision in firing will provide clues as to the types of ion channels which might be impacted by the pathological process.

Our findings are in rough agreement with a recent study on a mouse model of SCA1 engineered to express an 82 CAG repeat expansion under the control of the *Pcp2* promoter. The PC firing frequency in these mice is reduced at 5 weeks, an age at which rotarod performance and eyeblink conditioning are impaired but there is no sign of altered cerebellar morphology or PC loss (22). These findings were linked to larger A-type potassium currents and reduced glutamate receptor-mediated synaptic input.

The PC firing frequency was also reduced in a triplet repeat model of SCA3 (23), but this reduction likely occurs by a different pathophysiological mechanism. In this model, PCs are silenced as a result of excessive depolarization and consequent block of electrogenesis. The authors suggest that this silencing results from alterations in the kinetics of voltage-gated potassium channels (23).

Studies of other models of ataxia have reported more subtle changes in PC electrophysiology. Point mutations in the $K_v1.1$ channel lead to episodic ataxia type 1 (46), while mutations and triplet repeat expansions in P/Q- type voltage-gated calcium channels result in EA-2 (24) and in SCA6 (47), respectively. As mentioned above, reductions in voltage-gated calcium influx are found in a mouse

model of EA-2 and these reductions lead to less regular PC pacemaking. A positive modulator of calcium-activated potassium channels restores regular firing and ameliorates ataxic symptoms in these models, indicating that the pattern as well as the rate of PC firing likely impact motor coordination.

Finally, a recent study described a profound impairment in motor behavior and degradation in both the rate and regularity of PC firing in a mouse in which the RNA splicing factors RbFox1 and 2 had been deleted selectively from PCs ([48]). Intriguingly, RbFox1 was initially identified and named ataxin2-binding protein1 based on a yeast 2 hybrid screen using ataxin2 protein as bait ([28]). The PC-specific double-mutant animals showed dysregulation of RNA splicing for a number of ion channel transcripts known to be implicated in PC pacemaking. The data discussed in this report, however, suggest that mutant $ATXN2^{Q127}$ is not exerting its toxic effect on PC pacemaking via association with Rbfox1. Interestingly, in the mouse model presented here, we observe slowed pacemaking, yet with little variation between the WT and mutant mice across age. In the Rbfox 1 and 2, KO mouse model variation of the firing frequency was significantly higher than WT animals. Along with our RT-PCR splice variant data, this provides yet another piece of evidence that our animal model of SCA2 is working by way of a mechanism independent of downstream ion channel splice variants.

These studies highlight a range of proposed pathogenic mechanisms of expanded repeat alleles of *ATXN2*. Our physiological results are consistent with broad mechanisms of mRNA dysregulation, particularly if they result in changes to ion channel proteins involved in pacemaking. It is also possible that $ATXN2^{Q127}$ interacts with specific ion channel proteins required for pacemaking, explaining the reduction in this canonical physiological behavior of PCs.

Although loss of specific functions in neurodegenerative diseases is often attributed to loss of neurons, there is evidence that some manifestations of these diseases reflect alterations in neuronal function rather than morphological changes such as neuronal atrophy and loss. For Huntington disease, another polyglutamine disorder, early disease stages may result more from dysfunction than cell death as shown by recent electrophysiological studies in YAC mice ([49]). For polyQ ataxias, this has been supported in an animal model of SCA1, where behavioral and physiological changes clearly preceded PC loss and reduction in dendritic volume ([22]). In humans, mutations in *KCNC3* ($K_v3.3$) which are predicted to alter PC firing can lead to progressive cerebellar degeneration ([50,51]). Our studies using an SCA2 mouse model support this notion and show that the earliest changes in motor behavior are paralleled by changes in gene expression and PC firing, whereas reductions in molecular layer thickness and PC number follow much later.

MATERIALS AND METHODS

Animals

Transgenic mouse lines were generated using the pGEM construct containing the complete human ataxin-2 cDNA encoding 127 glutamine repeats (Q127) under the control of the Pcp2 promoter. Constructs were injected into oocytes of B6D2F1 mice; positive founders were backcrossed to WT animals of the same hybrid strain, which were used in all experiments. Mice were housed in a 12/12 h light on–off controlled room: lights on at 0600, with a constant temperature maintained at 20°C. Animals were housed (4 to 5 per cage) in clear Plexiglas hanging cages (30 × 18 × 15 cm) with HEPA-filtered air forced through barrier protective lids. All animals had *ad libitum* access to food (Lab Diet 5001) throughout the course of the study, except when being tested on the accelerating rotarod (~90 min per day). WT and transgenic ($ATXN2^{Q127}$) mice were age and weight matched for each experiment. Only trained personal handled the mice and all procedures carried out were in accordance with federal guidelines as well as University of Utah and UCLA IACUC approved protocols.

Behavioral analysis

Accelerating rotarod: cohorts were age and weight matched prior to all behavioral experiments. Male and female mice performed equally well; therefore, data were pooled and gender differences were not evaluated further. One day prior to testing, mice were placed on the rod rotating at a modest 10 revolutions per minute (rpm) for 2 min in order to acclimate the animals to the apparatus. Training was conducted over the course of 2 days. The third consecutive day of accelerating rotarod exposure served as the test day. Testing data consisted of the average of three trials. All mice were naive to the task at the beginning of testing. On the first day of training, animals were placed on the rod moving at 4 rpm. Over the course of 600 s, the rotational speed smoothly accelerated to 40 rpm and the latency to fall was recorded for each animal. Once the animal fell from the apparatus it was immediately returned to its home cage. A resting period lasting between 20 and 30 min was permitted between trials in order to allow for possible fatigue recovery.

Immunohistochemistry

Mice were deeply anesthetized with isoflurane, then transcardially perfused with ice-cold phosphate buffered saline (PBS). Tissue was quickly removed and immediately submerged into cold 4% paraformaldehyde (Electron Microscopy Sciences) and kept at 4°C overnight. The following day, PFA was replaced with 10 mM sodium citrate pH 6.0, and again incubated at 4°C overnight, after which the tissue was exposed to microwave radiation three times in10 s bursts. Following microwave radiation, tissues were cryoprotected by first incubating in 20% sucrose in PBS overnight followed by 30% sucrose overnight both at 4°C. After cryoprotection, the samples were suspended at optimal cutting temperature (Sakura Finetek) and kept at −80°C until the time of sectioning. Tissue sections were cut into 20 μM thick slices and floated into cold PBS. Tissues were washed three times for 15 min each wash at room temperature (RT) in PBS. A blocking/permeabilization solution consisting of 5% skim milk and 0.3% Triton in PBS was left on for 4 h at RT. Following removal of blocking solution, primary antibodies in wash

solution were incubated with the tissue slices. Primary antibodies used were as follows: Custom-designed ATXN2 rabbit polyclonal antibody targeted against the EKSTESSSGPKREE epitope sequence common to both humans and mice (SCA2-280), monoclonal mouse anti-calbindin-28k (Sigma). After 18 h incubation at 4°C, excess primary antibodies were removed using wash solution three times at 15 min each. DyLight-488 (green) and DyLight-550 (Red) (Thermo Fischer Scientific) fluorescent secondary antibodies were then incubated with the tissue for 2 h at RT. A final three washes, each 15 min in duration, were used to remove the residual secondary antibody and finally followed by a 5 min wash using 4',6-diamidino-2-phenylindole (408 nm, blue). Tissue was transferred to Superfrost Plus microscope slides (Fischer Scientific) and fixed in place with Prolong Gold (Invitrogen). Quantitative data were taken from three slices of each of two to three animals per genotype per age point.

Cell counting on calbindin 28K-stained sections was performed by three independent persons blinded to both the age and genotype. Counting was performed with images made from the 'Fissura Prima' between lobes V and VI along the mid-sagittal plane. PC counts were averaged between raters for three separate animals per genotype per age. The molecular layer thickness was determined using Nikon EZ-C1 confocal microscope software. Measurements were taken from the primary fissure comprised of lobes V and VI, measuring from the apex of the PC layer to the distal edge of the dendrites; N = three samples from each age and genotype.

Quantitative PCR

Mice were deeply anesthetized with isoflurane, and cerebella were removed and immediately submerged in liquid nitrogen. Tissues were kept at −80°C until the time of processing. RNA was extracted using the Ambion RNA extraction kit (Invitrogen) and cDNA synthesized using the QuantiTect Reverse Transcription kit (Qiagen). Diluted in RNA storage solution buffer (Invitrogen), cDNA samples were amplified with the Power SYBR Green PCR Master Mix chemistry (Applied Biosystems) and run on a Bio-Rad CFX96 qPCR machine (Bio-Rad). Primers were designed to amplify across exon/exon boundaries in order to minimize the amplification of potential contaminating genomic DNA. Each sample was repeated in quadruplicate and averaged for statistical comparisons. Within the quadruplicate repeats, false data were removed in accordance with the guidelines set forth using the Dixons Q-test of Outliers. All gene expression values were normalized to the pan-neuronal housekeeping gene *Wasf1*. Primer pairs designed for qPCR are given as forward and reverse, respectively:

Wasf1: (CCACCCTGCCTGTAATCAGT; GTTTTCAAT
   CCGCTCGTGTT);
h*ATXN2:* (AAGATATGGACTCCAGTTATGCAAA; CAAA
   GCCTCAAGTTCCTCAT);
m*Atxn2:* (AAGATACAGACTCCAGTTATGCACGG; GCT
   CCAGGTCCTTCTCCTTGTGC);
Pcp2: (ACAGTTAATTCCCTGCCTGG; CTCAAGGAGCTT
   GTGTCTGG);

Calb1: (GATTGGAGCTATCACCGGAA; TTCCTCGCAGG
   ACTTCAGTT);
Grm1: (TTCCTCAACATTTTCCGGAGAA; ACATGTGCC
   GACGGACACT);
Grid2: (GTTGGTCTCGACCTGGGAC; CTGTGCGGAATA
   CTTCATCATCT);
Ppp3ca: (CGTTCCATTTCCACCAAGTCAC; GCCTGCCC
   TCCTTCATGAGAT);
Gad1: (GGCATCTTCCACTCCTTC; GACGACTCTTCTCT
   TCCAG);
Cacna1a: (CCACCCTGCCTGTAATCAGT; GGAAGAATC
   TCGGGTGAGGTAC);
Itpr1: (GATGCTAAAGAGGGACAGAAGG; GCAGCGGA
   GAATGAGATCAAC).

Electrophysiology

Parasagittal cerebellar slices were made as described earlier ([52]). In brief, age-matched WT and *ATXN2^{Q127}* mice were anesthetized using isoflurane and decapitated in accordance with the protocol approved by the University of California Los Angeles Institutional Animal Care and Use Committee. The cerebellum was quickly dissected and placed in ice-cold extracellular solution (with composition in mm: 119 NaCl, 26 NaHCO$_3$, 11 glucose, 2.5 KCl, 2.5 CaCl$_2$, 1.3 MgCl$_2$ and 1 NaH$_2$PO$_4$, pH 7.4 when gassed with 5% CO$_2$ and 95% O$_2$). Parasagittal cerebellar slices (285–300 μm thickness) were made using a vibratome (Leica VT1000). The slices were incubated at 35°C for 30 min and stored at RT until use. Extracellular recordings were made from cerebellar slices placed in a heated recording chamber where the temperature is maintained at 34.5 ± 1°C using a dual channel heater controller (Model TC-344B, Warner Instruments) and constantly perfused with carbogen-bubbled extracellular solution at a rate of 2.8–3 ml per min. PCs were visualized using infrared differential interference contrast optics with an upright microscope (Leica) using ×40 water immersion objective. Recordings were made with borosilicate glass pipettes with resistances between 1 and 3 MΩ when filled with extracellular solution. To record action potential-associated capacitative current transients, the pipette potential was held at 0 mV and placed close to the axon hillock (soma/axon) of a Purkinje neuron. Recordings were made using Axon amplifiers 200B or 700B (Axon Instruments) in voltage-clamp mode. Currents were filtered at 2 kHz and sampled at 10 kHz using a Digidata 1440 (Axon Instruments). Spike detection and analysis were either carried out in pClamp 10 or with routines written in Igor (TaroTools, Dr Taro Ishikawa, https://sites.google.com/site/tarotoolsregister) and further analysis was performed using Excel or Igor software. Figures were made in Igor. The results are reported as mean ± SEM. Two minute duration extracellular recordings were collected from 50–120 PCs from two to seven mice for each genotype and age, and the experimenter was blinded to the genotype.

RT-PCR

RNA was isolated from mouse cerebellar tissue and transformed to cDNA as previously described (see above). Young 4 week and older 24 week samples from both WT (N = 3,

$N = 3$) and $ATXN2^{Q127}$ ($N = 3$, $N = 3$) mice were examined with primers designed to detect splice variant formations defined as 300 bp upstream and downstream from the (U)GCAUG alternative exon motif (48). Using HotStar Taq Plus (Qiagen), thermocycler conditions employed an annealing temperature of $60°C$ repeated for 30 cycles. The resultant product was visualized with ethidium bromide on a 2% agrose gel. Primers for *Cacna1B*, *Kcnd3* and *Kcnq2* amplified two endogenous bands. In these cases, samples were repeated in triplicate and analyzed for intra-sample band intensity using Kodak Molecular Imaging Software (v 5.0.1.27). The values were obtained by taking a ratio of the upper band to the lower band. The resultant ratios were log transformed and averaged for statistical comparisons between WT and $ATXN2^{Q127}$ mice. The primer sequence is given as forward and reverse, respectively:

Cacna1B: (GATGGAAGAAGCAGCCAATC; ACGCAGAT TCTGGAGCCTTA);
Cacna1D: (CCCAATGGAGGCATCACT; CTTCCAGCTGC TGTTTTTCC);
Cacna1S: (TTTGGAGATCCTTGGAATGTG; AGTCTCAT GACCCGGAACAG);
Kcnd3: (GGCAAGACCACCTCACTCA; ACTGGCTGGAC AGAGAAGGA);
Kcnq2: (CCCTGAAAGTCCAAGAGCAG; CTCCAGCTGG TTCAGAGGTG);
Scn8a (5): (GACCCGTGGAACTGGTTAGA; TCCAGATAG CTCTCGTTGAAGTT);
Scn8a (18): (AAATGGACAGCCTATGGCTTC; TCACCTC GTCGATTTCGAACCG).

Statistics

Two-factor ANOVA followed by Bonferonni *post-hoc* tests corrected for multiple comparisons at each age was used to compare between genotypes and across age for rotarod, cerebellar morphology and PC firing analysis. For qPCR and RT-PCR analysis, Student's two-tailed *t*-test was performed on data comparing $ATXN2^{Q127}$ and WT gene expression within each age group.

REFERENCES

1. Pulst, S.M., Nechiporuk, A., Nechiporuk, T., Gispert, S., Chen, X. N., Lopes-Cendes, I., Pearlman, S., Starkman, S., Orozco-Diaz, G., Lunkes, A. *et al.* (1996) Moderate expansion of a normally biallelic trinucleotide repeat in spinocerebellar ataxia type 2. *Nat. Genet.*, **14**, 269–276.
2. Pulst, S.M., Santos, N., Wang, D., Yang, H., Huynh, D., Velazquez, L. and Figueroa, K.P. (2005) Spinocerebellar ataxia type 2: polyQ repeat variation in the CACNA1A calcium channel modifies age of onset. *Brain*, **128**, 2297–2303.
3. van de Warrenburg, B.P., Hendriks, H., Durr, A., van Zuijlen, M.C., Stevanin, G., Camuzat, A., Sinke, R.J., Brice, A. and Kremer, B.P. (2005) Age at onset variance analysis in spinocerebellar ataxias: a study in a Dutch–French cohort. *Ann. Neurol.*, **57**, 505–512.
4. Servadio, A., Koshy, B., Armstrong, D., Antalffy, B., Orr, H.T. and Zoghbi, H.Y. (1995) Expression analysis of the ataxin-1 protein in tissues from normal and spinocerebellar ataxia type 1 individuals. *Nat. Genet.*, **10**, 94–98.
5. Banfi, S., Servadio, A., Chung, M., Capozzoli, F., Duvick, L.A., Elde, R., Zoghbi, H.Y. and Orr, H.T. (1996) Cloning and developmental expression analysis of the murine homolog of the spinocerebellar ataxia type 1 gene (Sca1). *Hum. Mol. Genet.*, **5**, 33–40.
6. Koeppen, A.H. (2005) The pathogenesis of spinocerebellar ataxia. *Cerebellum*, **4**, 62–73.
7. Zoghbi, H.Y. (1995) Spinocerebellar ataxia type 1. *Clin. Neurosci.*, **3**, 5–11.
8. Kiehl, T.R., Shibata, H. and Pulst, S.M. (2000) The ortholog of human ataxin-2 is essential for early embryonic patterning in C. elegans. *J. Mol. Neurosci.*, **15**, 231–241.
9. Aguiar, J., Fernandez, J., Aguilar, A., Mendoza, Y., Vazquez, M., Suarez, J., Berlanga, J., Cruz, S., Guillen, G., Herrera, L. *et al.* (2006) Ubiquitous expression of human SCA2 gene under the regulation of the SCA2 self-promoter cause specific Purkinje cell degeneration in transgenic mice. *Neurosci. Lett.*, **392**, 202–206.
10. van de Loo, S., Eich, F., Nonis, D., Auburger, G. and Nowock, J. (2009) Ataxin-2 associates with rough endoplasmic reticulum. *Exp. Neurol.*, **215**, 110–118.
11. Huynh, D.P., Scoles, D.R., Nguyen, D. and Pulst, S.M. (2003) The autosomal recessive juvenile Parkinson disease gene product, parkin, interacts with and ubiquitinates synaptotagmin XI. *Hum. Mol. Genet.*, **12**, 2587–2597.
12. Nonhoff, U., Ralser, M., Welzel, F., Piccini, I., Balzereit, D., Yaspo, M.L., Lehrach, H. and Krobitsch, S. (2007) Ataxin-2 interacts with the DEAD/ H-box RNA helicase DDX6 and interferes with P-bodies and stress granules. *Mol. Biol. Cell*, **18**, 1385–1396.
13. Kiehl, T.R., Nechiporuk, A., Figueroa, K.P., Keating, M.T., Huynh, D.P. and Pulst, S.M. (2006) Generation and characterization of Sca2 (ataxin-2) knockout mice. *Biochem. Biophys. Res. Commun.*, **339**, 17–24.
14. Lastres-Becker, I., Rub, U. and Auburger, G. (2008) Spinocerebellar ataxia 2 (SCA2). *Cerebellum*, **7**, 115–124.
15. McCann, C., Holohan, E.E., Das, S., Dervan, A., Larkin, A., Lee, J.A., Rodrigues, V., Parker, R. and Ramaswami, M. (2011) The ataxin-2 protein is required for microRNA function and synapse-specific long-term olfactory habituation. *Proc. Natl Acad. Sci. USA*, **108**, 655–662.
16. Ciosk, R., DePalma, M. and Priess, J.R. (2004) ATX-2, the C. elegans ortholog of ataxin 2, functions in translational regulation in the germline. *Development*, **131**, 4831–4841.
17. Satterfield, T.F. and Pallanck, L.J. (2006) Ataxin-2 and its Drosophila homolog, ATX2, physically assemble with polyribosomes. *Hum. Mol. Genet.*, **15**, 2523–2532.
18. Nonis, D., Schmidt, M.H., van de Loo, S., Eich, F., Dikic, I., Nowock, J. and Auburger, G. (2008) Ataxin-2 associates with the endocytosis complex and affects EGF receptor trafficking. *Cell. Signal.*, **20**, 1725–1739.
19. Satterfield, T.F., Jackson, S.M. and Pallanck, L.J. (2002) A Drosophila homolog of the polyglutamine disease gene SCA2 is a dosage-sensitive regulator of actin filament formation. *Genetics*, **162**, 1687–1702.
20. Palay, S.L. and Chan-Palay, V. (1974) *Cerebellar Cortex: Cytology and Organization*. Springer Verlag, NY.
21. Hausser, M. and Clark, B.A. (1997) Tonic synaptic inhibition modulates neuronal output pattern and spatiotemporal synaptic integration. *Neuron*, **19**, 665–678.

22. Hourez, R., Servais, L., Orduz, D., Gall, D., Millard, I., de Kerchove 'Exaerde, A., Cheron, G., Orr, H.T., Pandolfo, M. and Schiffmann, S.N. (2011) Aminopyridines correct early dysfunction and delay neurodegeneration in a mouse model of spinocerebellar ataxia type 1. *J. Neurosci.*, **31**, 11795–11807.

23. Shakkottai, V.G., do Carmo Costa, M., Dell'Orco, J.M., Sankaranarayanan, A., Wulff, H. and Paulson, H.L. (2011) Early changes in cerebellar physiology accompany motor dysfunction in the polyglutamine disease spinocerebellar ataxia type 3. *J. Neurosci.*, **31**, 13002–13014.

24. Walter, J.T., Alvina, K., Womack, M.D., Chevez, C. and Khodakhah, K. (2006) Decreases in the precision of Purkinje cell pacemaking cause cerebellar dysfunction and ataxia. *Nat. Neurosci.*, **9**, 389–397.

25. Huynh, D.P., Figueroa, K., Hoang, N. and Pulst, S.M. (2000) Nuclear localization or inclusion body formation of ataxin-2 are not necessary for SCA2 pathogenesis in mouse or human. *Nat. Genet.*, **26**, 44–50.

26. Raman, I.M. and Bean, B.P. (1999) Ionic currents underlying spontaneous action potentials in isolated cerebellar Purkinje neurons. *J. Neurosci.*, **19**, 1663–74.

27. Wulff, P., Schonewille, M., Renzi, M., Viltono, L., Sassoe-Pognetto, M., Badura, A., Gao, Z., Hoebeek, F.E., van Dorp, S., Wisden, W. *et al.* (2009) Synaptic inhibition of Purkinje cells mediates consolidation of vestibulo-cerebellar motor learning. *Nat. Neurosci.*, **12**, 1042–1049.

28. Shibata, H., Huynh, D.P. and Pulst, S.M. (2000) A novel protein with RNA-binding motifs interacts with ataxin-2. *Hum. Mol. Genet.*, **9**, 1303–1313.

29. Gehman, L.T., Stoilov, P., Maguire, J., Damianov, A., Lin, C.H., Shiue, L., Ares, M., Mody, I. and Black, D.L. (2011) The splicing regulator Rbfox1 (A2BP1) controls neuronal excitation in the mammalian brain. *Nat. Genet.*, **43**, 706–711.

30. Airaksinen, M.S., Eilers, J., Garaschuk, O., Thoenen, H., Konnerth, A. and Meyer, M. (1997) Ataxia and altered dendritic calcium signaling in mice carrying a targeted null mutation of the calbindin D28k gene. *Proc. Natl Acad. Sci. USA*, **94**, 1488–1493.

31. Vig, P.J., Subramony, S.H., Burright, E.N., Fratkin, J.D., McDaniel, D.O., Desaiah, D. and Qin, Z. (1998) Reduced immunoreactivity to calcium-binding proteins in Purkinje cells precedes onset of ataxia in spinocerebellar ataxia-1 transgenic mice. *Neurology*, **50**, 106–113.

32. Schwaller, B., Meyer, M. and Schiffmann, S. (2002) 'New' functions for 'old' proteins: the role of the calcium-binding proteins calbindin D-28k, calretinin and parvalbumin, in cerebellar physiology. *Cerebellum*, **1**, 241–258.

33. Bidaud, I., Mezghrani, A., Swayne, L.A., Monteil, A. and Lory, P. (2006) Voltage-gated calcium channels in genetic diseases. *Biochim. Biophys. Acta*, **1763**, 1169–1174.

34. Felix, R. (2000) Channelopathies: ion channel defects linked to heritable clinical disorders. *J. Med. Genet.*, **37**, 729–740.

35. Vig, P.J., Wei, J., Shao, Q., Lopez, M.E., Halperin, R. and Gerber, J. (2012) Suppression of calbindin-D28k expression exacerbates SCA1 phenotype in a disease mouse model. *Cerebellum*, **11**, 718–732.

36. Liu, J., Tang, T.S., Tu, H., Nelson, O., Herndon, E., Huynh, D.P., Pulst, S.M. and Bezprozvanny, I. (2009) Deranged calcium signaling and neurodegeneration in spinocerebellar ataxia type 2. *J. Neurosci.*, **29**, 9148–9162.

37. Bezprozvanny, I. and Hayden, M.R. (2004) Deranged neuronal calcium signaling and Huntington disease. *Biochem. Biophys. Res. Commun.*, **322**, 1310–1317.

38. Watase, K., Barrett, C.F., Miyazaki, T., Ishiguro, T., Ishikawa, K., Hu, Y., Unno, T., Sun, Y., Kasai, S., Watanabe, M. *et al.* (2008) Spinocerebellar ataxia type 6 knockin mice develop a progressive neuronal dysfunction with age-dependent accumulation of mutant CaV2.1 channels. *Proc. Natl Acad. Sci. USA*, **105**, 11987–11992.

39. Tang, T.S., Tu, H., Chan, E.Y., Maximov, A., Wang, Z., Wellington, C.L., Hayden, M.R. and Bezprozvanny, I. (2003) Huntingtin and huntingtin-associated protein 1 influence neuronal calcium signaling mediated by inositol-(1,4,5)-triphosphate receptor type 1. *Neuron*, **39**, 227–2239.

40. Schorge, S., van de Leemput, J., Singleton, A., Houlden, H. and Hardy, J. (2010) Human ataxias: a genetic dissection of inositol triphosphate receptor (ITPR1)-dependent signaling. *Trends Neurosci.*, **33**, 211–219.

41. Conquet, F., Bashir, Z.I., Davies, C.H., Daniel, H., Ferraguti, F., Bordi, F., Franz-Bacon, K., Reggiani, A., Matarese, V., Conde, F. *et al.* (1994) Motor deficit and impairment of synaptic plasticity in mice lacking mGluR1. *Nature*, **372**, 237–243.

42. Mandolesi, G., Cesa, R., Autuori, E. and Strata, P. (2009) An orphan ionotropic glutamate receptor: the delta2 subunit. *Neuroscience*, **158**, 67–77.

43. Motohashi, J., Kakegawa, W. and Yuzaki, M. (2007) Ho15J: a new hotfoot allele in a hot spot in the gene encoding the delta2 glutamate receptor. *Brain Res.*, **1140**, 153–160.

44. Zuo, J., De Jager, P.L., Takahashi, K.A., Jiang, W., Linden, D.J. and Heintz, N. (1997) Neurodegeneration in Lurcher mice caused by mutation in delta2 glutamate receptor gene. *Nature*, **388**, 769–773.

45. Katoh, A., Yoshida, T., Himeshima, Y., Mishina, M. and Hirano, T. (2005) Defective control and adaptation of reflex eye movements in mutant mice deficient in either the glutamate receptor delta2 subunit or Purkinje cells. *Eur. J. Neurosci.*, **21**, 1315–1326.

46. Browne, D.L., Gancher, S.T., Nutt, J.G., Brunt, E.R., Smith, E.A., Kramer, P. and Litt, M. (1994) Episodic ataxia/myokymia syndrome is associated with point mutations in the human potassium channel gene, KCNA1. *Nat. Genet.*, **8**, 136–140.

47. Zhuchenko, O., Bailey, J., Bonnen, P., Ashizawa, T., Stockton, D.W., Amos, C., Dobyns, W.B., Subramony, S.H., Zoghbi, H.Y. and Lee, C.C. (1997) Autosomal dominant cerebellar ataxia (SCA6) associated with small polyglutamine expansions in the alpha 1A-voltage-dependent calcium channel. *Nat. Genet.*, **15**, 62–69.

48. Gehman, L.T., Meera, P., Stoilov, P., Shiue, L., O'Brien, J.E., Meisler, M.H., Ares, M., Otis, T.S. and Black, D.L. (2012) The splicing regulator Rbfox2 is required for both cerebellar development and mature motor function. *Genes Dev.*, **26**, 445–460.

49. Milnerwood, A.J., Gladding, C.M., Pouladi, M.A., Kaufman, A.M., Hines, R.M., Boyd, J.D., Ko, R.W., Vasuta, O.C., Graham, R.K., Hayden, M.R. *et al.* (2010) Early increase in extrasynaptic NMDA receptor signaling and expression contributes to phenotype onset in Huntington's disease mice. *Neuron*, **65**, 178–190.

50. Waters, M.F., Minassian, N.A., Stevanin, G., Figueroa, K.P., Bannister, J.P., Nolte, D., Mock, A.F., Evidente, V.G., Fee, D.B. and Muller, U. (2006) Mutations in voltage-gated potassium channel KCNC3 cause degenerative and developmental central nervous system phenotypes. *Nat. Genet.*, **38**, 447–451.

51. Figueroa, K.P., Minassian, N.A., Stevanin, G., Waters, M., Garibyan, V., Forlani, S., Strzelczyk, A., Burk, K., Brice, A., Durr, A. *et al.* (2010) KCNC3: phenotype, mutations, channel biophysics—a study of 260 familial ataxia patients. *Hum. Mutat.*, **31**, 191–196.

52. Meera, P., Wallner, M. and Otis, T.S. (2011) Molecular basis for the high THIP/gaboxadol sensitivity of extrasynaptic GABA(A) receptors. *J. Neurophysiol.*, **106**, 2057–2064.